surements will be reported in detail elsewhere.

Finally, one could question the physiological relevance of these experiments and observations. However, Pr^{3+} is an often-used Ca^{2+} substitute.[43] Also, and although free-acid acids are minor components of biological membranes, exogeneous additions alter several membrane-mediated cellular functions such as cell permeability[44] or activity of membrane-bound enzymes.[45-47] Furthermore, free fatty acids can be formed within the membrane by the action of phospholipases.

To sum up, the increase of Pr^{3+} translocation across phosphatidylcholine vesicles by lasalocid A, as induced by the single adjunction of lauric acid, finds its most likely explanation in participation of the fatty acid in the proton countertransport. Such a cation-proton antiport process could be used to model cation-proton exchanger systems in biological membranes.[47-50]

Registry No. X-537A, 25999-31-9; Pr, 7440-10-0; H^+, 12408-02-5; Na, 7440-23-5; lauric acid, 143-07-7.

(43) Mikkelson, R. B. In *Biological Membranes*; Chapman, D., Wallach, D. F. H., Eds.; Academic: London, 1976; pp 153-190.
(44) Schram, N.; Eisenkraft, B.; Barkai, E. *Biochim. Biophys. Acta* **1967**, *135*, 44-52.
(45) Schmalzig, G.; Kutchera, P. *J. Membr. Biol.* **1982**, *69*, 65-76.
(46) Rhoads, D. E.; Peterson, N. A.; Raghupathy, E. *Biochemistry* **1982**, *21*, 4782-4787.
(47) Pieper, G. M.; Salhany, J. M.; Murray, W. J.; Wu, S. T.; Eliot, R. S. *Biochim. Biophys. Acta* **1984**, *803*, 229-240.
(48) Bassalina, M.; Damanio, E.; Leblanc, G. *Biochemistry* **1984**, *23*, 5288-5294.
(49) Nakamura, T.; Tokuda, H.; Unemoto, T. *Biochim. Biophys. Acta* **1984**, *776*, 330-336.
(50) Kinsella, J. L.; Aronson, P. S. *Am. J. Physiol.* **1980**, *238*, 461-469.

ENDOR of the Resting State of Nitrogenase Molybdenum-Iron Proteins from *Azotobacter vinelandii*, *Klebsiella pneumoniae*, and *Clostridium pasteurianum*: ^{1}H, ^{57}Fe, ^{95}Mo, and ^{33}S Studies

Ronald A. Venters,[1a] Mark J. Nelson,[1b] Paul A. McLean,[1c] Anne E. True,[1d] Mark A. Levy,[1e] Brian M. Hoffman,*[1d] and William H. Orme-Johnson*[1c]

Contribution from the Department of Chemistry, Northwestern University, Evanston, Illinois 60201, and Department of Chemistry, Massachusetts Institute of Technology, Cambridge, Massachusetts 02139. *Received August 19, 1985*

Abstract: Electron nuclear double resonance (ENDOR) studies of native and isotopically enriched MoFe proteins hold the promise of individually characterizing every atom of the catalytically active FeMo-co cluster of the nitrogenase MoFe protein. This report presents ^{1}H, ^{57}Fe, $^{95,97}Mo$, and ^{33}S ENDOR measurements in a comparison of the MoFe protein isolated from the three titled organisms, Avl, Kpl, and Cpl. We have examined in detail single-crystal-like ^{57}Fe resonances from at least five distinct iron sites in each of the three enzymes, revising somewhat our earlier assignments. The analysis incidentally gives the electron spin zero-field splitting parameters to high precision. ^{95}Mo ENDOR measurements for Cpl and Kpl give ^{95}Mo hyperfine and quadrupole coupling constants. They indicate that a single molybdenum is integrated into the MoFe spin system and that the molybdenum is most plausibly viewed as being in an even-electron state, which may be assigned provisionally as unsymmetrically coordinated Mo^{IV}. The observation of an exchangeable proton or protons from each protein source suggests a site on the cluster accessible to solvent and perhaps containing H_2O or OH^-. Cpl enriched in ^{33}S gives the first observed ENDOR signals from this nucleus. The resonances from ^{33}S are assignable to the inorganic sulfur because, it is argued, the FeMo-co cluster must be bound to the protein primarily, if not exclusively, by residues other than cysteinyl.

Nitrogenase comprises two extremely oxygen-sensitive metalloproteins, the iron protein (Fe protein) and the molybdenum-iron protein (MoFe protein).[2] The Fe protein accepts electrons from oxidative processes operating at or below -0.4 V and then specifically passes them on to the MoFe protein for use in the reduction of dinitrogen and other substrates.[3] The MoFe protein as isolated from *Azotobacter vinelandii* (Avl),[4] *Clostridium pasteurianum* (Cpl),[5,6] and *Klebsiella pneumoniae* (Kpl)[7] is an $\alpha_2\beta_2$ tetramer with molecular weights of approximately 240 000 for Avl and 220 000 for both Cpl and Kpl. Chemical analysis of the MoFe protein has shown it to contain 2 mol of molybdenum, approximately 30 mol of iron, and approximately 30 mol of acid-labile sulfur/mol of peptide component.[8]

Accurate chemical and spectroscopic assignment of these molybdenum, iron, and sulfur atoms into individual clusters and investigation of the structure of those clusters constitute much of the recent progress in the study of nitrogenase. In particular,

(1) (a) Northwestern University. Present address: Benger Laboratory, E. I. du Pont de Nemours and Co., Waynesboro, VA 22980. (b) Massachusetts Institute of Technology. Present address: Experimental Station, E. I. du Point de Nemours and Co., Wilmington, DE 19898. (c) Massachusetts Institute of Technology. (d) Northwestern University. (e) Massachusetts Institute of Technology. Present address: Smith Kline and French Laboratories, Philadelphia, PA 19101.
(2) The following abbreviations are used: Avl, Kpl, and Cpl, the molybdenum-iron proteins, respectively, from *A. vinelandii*, *K. pneumoniae*, and *C. pasteurianum*; MoFe, molybdenum-iron protein; FeMo-co, molybdenum-iron cofactor; ENDOR, electron nuclear double resonance.
(3) (a) Orme-Johnson, W. H. *Annu. Rev. Biophys. Chem.* **1985**, *14*, 419-459. (b) Nelson, M. J.; Lindahl, P. A.; Orme-Johnson, W. H. In *Advances in Inorganic Biochemistry*; Eichorn, G. L., Marzilli, L. G., Eds.; Elsevier: New York, 1981; 1-40. (c) Mortenson, L. E.; Thorneley, R. N. F. *Annu. Rev. Biochem.* **1979**, *48*, 387-418. (d) Brill, W. J. *Microbiol. Rev.* **1980**, *44*, 449-467. (e) Yates, M. G. *Biochem. Plants* **1980**, *5*, 1-64. (f) Robson, R. L.; Postgate, J. R. *Annu. Rev. Microbiol.* **1980**, *34*, 183-207.
(4) Shah, V. K.; Davis, L. C.; Brill, W. J. *Biochim. Biophys. Acta* **1972**, *256*, 498-511.
(5) Nakos, G.; Mortenson, L. E. *Biochim. Biophys. Acta* **1971**, *229*, 431-436.
(6) Zumft, W. G.; Hase, T.; Matsubara, H. In *Molybdenum Chemistry of Biological Significance*; Newton, W. E., Otsuka, S., Eds.; Plenum: New York, 1980; p 59-72.
(7) Eady, R. R.; Smith, B. E.; Cook, K. A.; Postgate, J. R. *Biochem. J.* **1972**, *128*, 655-675.
(8) Davis, L. C.; Shah, V. K.; Brill, W. J.; Orme-Johnson, W. H. *Biochim. Biophys. Acta* **1972**, *256*, 512-523.

0002-7863/86/1508-3487$01.50/0

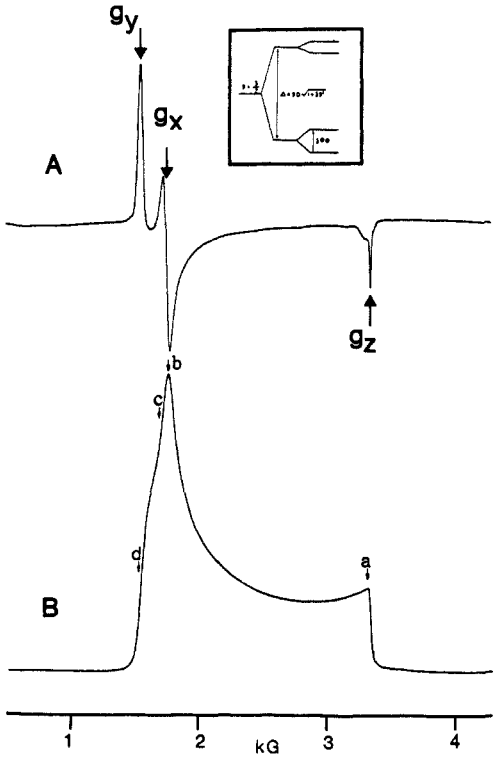

Figure 1. EPR spectra of *A. vinelandii* MoFe protein of nitrogenase (Avl) taken at 2 K: (A) absorption derivative; (B) rapid-passage dispersion. Positions at the extreme edges of the EPR spectrum, near either g_z' (position a) or g_y' (position d) give single-crystal-like ENDOR patterns. Positions such as c and b (g_x') involve a well-defined range of molecular orientations. Conditions: microwave power, 0.063 mW; 100-kHz field modulation, 4 G.

the MoFe protein exhibits an unusual EPR spectrum (Figure 1) with apparent g values of ca. 4.3, 3.6, and 2, depending on the species, at temps. below 25 K.[8-12] This EPR spectrum is derived from the ground-state Kramers' doublet of an $S = {}^3/_2$ multimetal center (Figure 1, inset), associated with enzyme-bound molybdenum–iron cofactor (FeMo-co). Extensive efforts have been made to characterize this EPR-active center because there is evidence that these clusters are in the active site of the enzyme. For example, recent studies of *nifV*⁻ mutants of *K. pneumoniae* reveal that a mutation restricted to the cofactor alters the substrate-reducing properties.[3a] Careful analytical studies have narrowed the range of stoichiometry of wild-type cofactor cluster to $MoFe_{6-8}S_{9\pm1}$.[13,14] The structure of this material is unknown but is under active investigation. The first evidence regarding the stoichiometry and detailed electronic properties of FeMo-co was obtained through Mössbauer spectroscopy. Analysis of the component of the Mössbauer spectrum that corresponds to the EPR-active FeMo-co entity indicated that this cluster includes six spin-coupled iron atoms and obtained values for their hyperfine interaction constants.[15] EXAFS measurements give average properties of the iron sites and have been used to characterize the local environment of molybdenum.[16,17]

The present report describes our continuing use of electron nuclear double resonance (ENDOR) spectroscopy in examining the structure and properties of the MoFe protein in its resting state.[18,19] ENDOR spectroscopy is a nuclear magnetic resonance technique in which a nuclear transition at a site within a paramagnetic center is detected by its effect on the EPR signal of the center.[20] Unlike ordinary NMR, it is comparably easy to detect resonances from every nucleus with spin ($I > 0$). However, as an NMR technique it offers resolution that is orders of magnitude better than that of EPR, thus permitting the measurement of electron nuclear hyperfine interactions that are too small to observe in EPR. Moreover, it is possible to employ frozen-solution samples yet achieve orientation-selected ENDOR spectra and to extract from them single-crystal values through the theory of polycrystalline ENDOR patterns.[21]

ENDOR measurements of native and isotopically enriched MoFe proteins could in principle characterize every atom of the catalytically active FeMo-co cluster. This report, in fact, describes resonances from *each* type of atom known to be present in cofactor and compares MoFe enzymes, Avl, Kpl, and Cpl, isolated from three different organisms. We have examined in detail single-crystal-like resonances from at least five distinct iron sites in each of the three enzymes. ^{95}Mo ENDOR measurements for two proteins indicate that a single molybdenum is integrated into the MoFe spin system. The molybdenum is most plausibly viewed as being in an even-electron state and may be assigned provisionally as unsymmetrically coordinated Mo^{IV}. The observation of an exchangeable proton(s) from each protein source suuggests a site on the cluster accessible to solvent and coordinating H_2O or OH^-. MoFe protein enriched in ^{33}S gives the first observed ENDOR signals from this nucleus. This set of results provides the sharpest insight to date into the properties of the MoFe protein, highlights the similarities and differences among these three enzymes, and constitutes the framework for later examination of the interactions of substrates and inhibitors with the MoFe protein, as well as the influence of genetic alterations on the cofactor cluster.

Experimental Procedures

Sample Preparation. Isotopically enriched materials were obtained from Oak Ridge National Laboratories. ^{100}Mo (97.4%), ^{97}Mo (94.2%), and ^{95}Mo (96.5%) were obtained as the elemental powders. These were oxidized to MoO_3 in concentrated nitric acid at 100 °C overnight and then hydrolyzed by addition of concentrated ammonium hydroxide. The ammonium molybdate was precipitated by addition of ethanol, collected by centrifugation, washed with ethanol, and dried at 85 °C. Yields ranged from 90 to 100%. Ferric oxide (86.0% ^{57}Fe) was treated with concentrated hydrochloric acid to obtain the chloride. Elemental sulfur (25.5% ^{33}S) was oxidized to sulfuric acid in aqua regia. Some manipulations, including concentration of protein samples by ultrafiltration, were carried out in a Vacuum Atmospheres glovebox under helium. All solutions used in protein manipulations were degassed thoroughly by repetitive evacuation and flushing with argon. Activity assays were performed as published,[7,22] using protein concentrations determined by Biuret assay[23] or the Lowry method.[24] The reported pH of ENDOR

(9) Gillum, W. O.; Mortenson, L. E.; Chen, J. S.; Holm, R. H. *J. Am. Chem. Soc.* **1977**, *99*, 584–595.
(10) Münck, E.; Rhodes, H.; Orme-Johnson, W. H.; Davis, L. C.; Brill, W. J.; Shah, V. K. *Biochim. Biophys. Acta* **1975**, *400*, 32–53.
(11) Huynh, B. H.; Henzl, M. T.; Christner, J. A.; Zimmermann, R.; Orme-Johnson, W. H.; Münck, E. *Biochim. Biophys. Acta* **1980**, *623*, 124–138.
(12) Smith, B. E.; Lowe, D. J.; Bray, R. C. *Biochem. J.* **1972**, *130*, 641–643.
(13) Nelson, M. J.; Levy, M. A.; Orme-Johnson, W. H. *Proc. Natl. Acad. Sci. U.S.A.* **1983**, *80*, 147–150.
(14) Yang, S. S.; Pan, W. H.; Friesen, G. D.; Burgess, B. K.; Corbin, J. L.; Stiefel, E. I.; Newton, W. E. *J. Biol. Chem.* **1982**, *257*, 8042–8048.
(15) Huynh, B. H.; Münck, E.; Orme-Johnson, W. H. *Biochim. Biophys. Acta* **1979**, *576*, 192–203.
(16) (a) Cramer, S. P.; Hodgson, K. O.; Gillum, W. D.; Mortenson, L. E. *J. Am. Chem. Soc.* **1978**, *100*, 3398–3407. (b) Cramer, S. P.; Hodgson, K. O.; Gillum, W. D.; Mortenson, L. E.; Stiefel, E. I.; Chisnell, J. R.; Brill, W. J.; Shah, V. K. *J. Am. Chem. Soc.* **1978**, *100*, 3814–3838. (c) Newton, W. E.; Burgess, B. K.; Cummings, S. C.; Lough, S.; McDonald, J. W.; Rubinson, J. F.; Conradson, S. D.; Hodgson, K. O. In *Advances in Nitrogen Fixation Research*; Veeger, C., Newton, W F., Eds.; Nijoff: The Hague, 1984; p 160.
(17) Antonio, M. R.; Teo, B.-K.; Orme-Johnson, W. H.; Nelson, M. J.; Groh, S. E.; Lindahl, P. A.; Kauzlarich, S. M.; Averill, B. A. *J. Am. Chem. Soc.* **1982**, *104*, 4703–4705.
(18) Hoffman, B. M.; Roberts, J. E.; Orme-Johnson, W. H. *J. Am. Chem. Sc.* **1982**, *104*, 860–862.
(19) Hoffman, B. M.; Venters, R. A.; Roberts, J. E.; Nelson, M. J.; Orme-Johnson, W. H. *J. Am. Chem. Soc.* **1982**, *104*, 4711–4712.
(20) (a) Abragam, A.; Bleaney, B. *Electron Paramagnetic Resonance of Transition Ions*; Clarendon: Oxford, 1970. (b) Atherton, N. M. *Electron Spin Resonance*; Halstead: New York, 1973.
(21) (a) Hoffman, B. M.; Martinsen, J.; Venters, R. A. *J. Magn. Reson.*, 1984, *59*, 110–123. (b) Hoffman, B. M.; Martinsen, J.; Venters, R. A. *J. Magn. Reson.* **1985**, *62*, 537–542.
(22) Burgess, B. K.; Jacobs, D. B.; Stiefel, E. I. *Biochim. Biophys. Acta* **1980**, *614*, 196–209.

samples has been corrected to 0 °C to account for changes during freezing.

A. vinelandii OP (ATCC No. 13905) was grown in a fixed nitrogen-free medium containing 4.6 mM K_2HPO_4, 1.5 mM KH_2PO_4, 1.7 mM NaCl, 0.8 mM $MgSO_4$, 0.6 mM $CaCl_2$, 0.02 mM $FeSO_4$, 0.01 mM Na_2MoO_4, and 2% sucrose. Cultures (100 L) were aerated vigorously and monitored by measuring OD_{600} in a 1-cm cuvette. Cells were harvested in mid-log phase corresponding to OD_{600} between 1.2 and 1.5. The paste obtained from the Sharples centrifuge was frozen in liquid nitrogen and stored at −85 °C.

C. pasteurianum W6 was grown from spores provided by L.E. Mortenson in 18-L cultures with 0.2 mM Na_2SO_4 as previously described.[13] These cultures were sparged with nitrogen and harvested when OD_{600} was between 2.0 and 2.5. The Sharples centrifuge was flushed with nitrogen for 30 min before and after passage of the culture, and cells were transferred quickly to liquid nitrogen and stored at −85 °C.

K. pneumoniae M5al (gift of Dr. R. A. Dixon) was grown at 30 °C in 100-L cultures in NFDM[25a] except that $FeSO_4$ was replaced with iron citrate (30 mg/L) and glucose (2% w/v) replaced sucrose. Cultures were bubbled with N_2 gas at approximately 1.5–2 L/min. Cultures were inoculated with saturated cultures grown in 2.5 L of LB (^{95,100}Mo enrichment[25b]) or 10 L of NFDM + $(NH_4)_2SO_4$ at 1 g/L (^{57}Fe enrichment). In vivo C_2H_2 reduction activity was monitored, and cells were harvested when this activity had just past a peak (usually after 23–26 h). Cells were harvested and stored as for *Azotobacter* (above).

For enrichment with ^{57}Fe, concentrates of the phosphate and sucrose components of the medium were treated to remove contaminating iron as follows: To each concentrate was added 10 g/L of alumina (14–28 mesh), and the suspensions were autoclaved for 20 min. After they were stirred overnight at 30 °C, the suspensions were filtered twice through paper that had been treated with basic EDTA and then rinsed, yielding slightly turbid solutions. Potassium phosphate buffer for ^{57}Fe enrichment of Kpl was prepared by titrating KOH with phosporic acid to pH 7.4 to give a 2 M concentrate that was then autoclaved. All glassware used was soaked in 1 M hydrochloric acid.

For growth of *A. vinelandii*, approximately 1 μM $^{57}FeCl_3$ was added; for *C. pasteurianum* and *K. pneumoniae*, approximately 6 and 5 μM $^{57}FeCl_3$ was added in a 10-fold and 50% excess of citric acid adjusted to pH 7.5 with solid KOH, respectively. For enrichment of molybdenum, 5 μM enriched ammonium molybdate was added to the medium instead of the unenriched sodium molybdate; this is enough to swamp any molybdenum contaminants. For enrichment with ^{33}S (initial isotopic purity 25.5%), the protocol used previously for ^{35}S was followed.[13]

Molybdenum–iron protein from *A. vinelandii* was purified as published[22] with minor modifications. The molybdenum–iron protein from *C. pasteurianum* was purified as published,[13] except that the final Sepharose 6B column used previously was replaced by a Sephacryl S-200 column (2.5 × 108 cm) eluted with 0.1 M NaCl/0.05 M Tris-HCl, pH 8.0/2 mM $Na_2S_2O_4$ at 25 mL/h, and the order of the last two columns was reversed. Molybdenum–iron protein from *K. pneumonia* was purified as was that from *C. pasteurianum* except that the buffer was pH 7.4, the Sephacryl column buffer contained 0.2 M NaCl, and CO was left out of the column buffers.

Protein samples were exchanged into D_2O by repetitive 10-fold dilution with 30 mM TES-DCl, pD 7.2/2mM $Na_2S_2O_4$ in D_2O (Avl/Cpl) or Tris-DCl pD 7.4/2 mM $Na_2S_2O_4$ (Kpl) and concentration by ultrafiltration.

Samples were prepared anaerobically by loading the protein solutions into ENDOR tubes under argon and freezing in liquid nitrogen. The concentration (mg/mL) and specific activities (nmol of ethylene produced/min per mg) of the proteins used are as follows: Avl (30; 2100), Avl in D_2O (15; 2000), ^{57}Fe Avl (30; 2100), Cpl (40; 1900), Cpl in D_2O (45; 1800), ^{100}Mo Cpl (90; 2000), ^{97}Mo Cpl (60; 1700), ^{95} Mo Cpl (45; 1500), ^{33}S Cpl (80; 1800), ^{57}Fe Cpl (60; 1900), ^{100}Mo Kpl (80; 1760), ^{95}Mo Kpl (75; 1700) ^{57}Fe Kpl (70; 1650).

ENDOR Measurements. The ENDOR spectrometer is based on a Varian Associates E-109 EPR spectrometer. Experiments were performed with a silvered TE_{102} sample cavity held at $T \sim 2$ K in a Janis Corp. liquid helium immersion Dewar. Mutually perpendicular field-modulation and radiofrequency coils run through the cavity. The resonance frequency can be measured to better than 2 ppm by using a Sage Laboratories Model 251 tunable coherent synchronizer.

The ENDOR attachment is comprised of a Nicolet Model 1280E computer and 293B pulse programmer driving a Programmed Test Sources (PTS) Model 160 frequency synthesizer (0.1–160 MHz). The synthesizer has a stability of 10^{-8}/day, and thus frequencies reported here are effectively free from instrumental uncertainty. The output of the PTS is controlled by a homebuilt leveling circuit and is amplified by an Electronic Navigator Industries (ENI) Model A150 (0.3–35 MHz) or a 3200L (250 kHz–150 MHz) power amplifier. Radiofrequency power of 20 W gives ~1 G in the rotating frame.

The ENDOR signals were observed as an intensity change in the 100-kHz field-modulated, dispersion mode EPR signal and accumulated in the computer. Each ENDOR resonance was the subject of at least four independent measurements. The proton and iron resonances reported here have narrow line widths and were acquired with exceptionally good signal-to-noise. Because of this and the high accuracy of the frequency synthesizer, resonance frequencies could be measured with exceptional accuracy; in particular for ^{57}Fe, the uncertainties are ±0.01 MHz in most cases.

Table I. Electron Spin Hamiltonian Parameters for MoFe Proteins[a]

	$S' = {}^1/_2$ representation[b]		$S = {}^3/_2$ representation		
protein	g_y'	g_x'	$g_\perp$[c]	$\lambda^c = E/D$	$\Delta(2D)$,[d] cm^{-1}
Avl	4.320	3.681	2.005	0.053	12.2
Kpl	4.328	3.672	2.004	0.055	12.5
Cpl	4.306	3.798	2.028	0.042	10.5

[a] Samples in Tris-HCl buffer at pH 8.0 (avl, Kpl) or 8.6 (Cpl) (pH values corrected to 0 °C). [b] Uncertainties ±0.003. In each case, $g_{min}' = 2.01$. [c] Calculated from (g_y', g_x') by using eq 1. [d] $\Delta = 2D(1 + 3\lambda^2)^{1/2}$ calculated from ^{57}Fe ENDOR data according to eq 4 (see text); uncertainties ± 0.01 cm^{-1}. Because λ is small, within experimental error, $\Delta = 2D$.

Results

EPR. Figure 1A presents the 2K absorption derivative EPR spectrum, and Figure 1B presents the rapid-passage dispersion derivative EPR spectrum of a frozen solution of the molybdenum–iron protein (Avl) as isolated from *A. vinelandii* (dithionite reduced, pH 8.0); spectra for Cpl and Kpl are similar. The passage spectrum may be seen to correspond to the envelope of the polycrystalline EPR absorption spectrum of the MoFe protein. These spectra are associated with the lower, $m_s = \pm{}^1/_2$, doublet of a metal center with a total electron spin of $S = {}^3/_2$.[10] As such, they can be described in a representation based on a fictitious spin $S' = {}^1/_2$ characterized by a **g**′ tensor with principal values $g_y' = 4.32$, $g_x' = 3.68$, and $g_z' = 2.01$. The spin quartet is split into two Kramers' doublets (inset Figure 1), separated by the zero-field splitting energy $\Delta = 2D(1 + 3\lambda^2)^{1/2}$, where D and E are the axial and rhombic zero-field splitting parameters and the rhombicity is measured by $\lambda = E/D$; the g_z' axis corresponds to the direction of the axial (largest) component of the zero-field splitting tensor. Variable-temperature EPR studies gave a value of $\Delta \sim 12$ cm^{-1}.[15] By analysis of the g' values, the ratio of zero-field splitting parameters characterizing the rhombicity of the zero-field splitting tensor (λ) can be obtained, along with a value for $g_\perp$ in the $S = {}^3/_2$ representation, through inversion of eq 1.[26] Table I presents

$$g_{x,y}' = g_\perp\left[1 + \frac{1 \mp 3\lambda}{(1 + 3\lambda^2)^{1/2}}\right] \quad (1)$$

the values for λ and $g_\perp$ for the three molybdenum–iron proteins studied, as well as values of $2D$ obtained as described below. The electronic spin Hamiltonian parameters for Avl and Kpl are indistinguishable. However, the zero-field splitting and rhombicity of Cpl are significantly smaller whereas $g_\perp$ is larger.

ENDOR. For a single-crystal ENDOR measurement from a set of equivalent nuclei (n) of spin I one expects $4I$ ENDOR transitions (selection rules, $\Delta m_s = 0$ and $\Delta m_I = \pm 1$) having first-order transition frequencies[20]

$$\nu_{\pm(m_I)} = |\pm A^{N'}/2 + \nu_N + 3P^N(2m_I - 1)/2| \quad (2)$$

where $-I + 1 \leq m \leq I$ and $A^{N'}$ is the angle-dependent hyperfine

(23) Cooper, T. G. *The Tools of Biochemistry*; Wiley: New York, 1977; p 52.
(24) Lowry, O. H.; Rosebrough, N. J.; Farr, A. L.; Randall, R. J. *J. Biol. Chem.* **1951**, *193*, 265–275.
(25) (a) Cannon, F. C.; Dixon, R. A.; Postgate, J. R.; Primrose, S. B. *J. Gen. Microbiol.* **1974**, *80*, 227–239. (b) Miller, J. H. In *Experiments in Molecular Genetics*; Cold Spring Harbor Lab: Cold Spring Harbor, NY, 1972.
(26) Hoffman, B. M.; Weschler, C. J.; Basolo, F. *J. Am. Chem. Soc.* **1976**, *98*, 5473–5482.

coupling in the $S' = {}^1/_2$ representation. When the lower Kramers' doublet is treated as an $S' = {}^1/_2$ system, the principal axis values of the hyperfine interaction tensor, A_j', are related to the principal axis values of the hyperfine Hamiltonian in the $S = {}^3/_2$ representation A_j by the relationship

$$A_j' = A_j g_j'/g_j \tag{3}$$

when the electron Zeeman and hyperfine tensors are coaxial. The quadrupole splitting Hamiltonian for a nucleus of spin I is expressed in terms of a traceless tensor, $P_x^N + P_y^N + P_z^N = 0$, where $P_i^N = e^2q_iQ/[h2I(2I-1)]$; the angle-dependent quadrupole splitting constant of eq 2, P^N, is specified so that $P_i^N = P^N$ for a principal axis direction. Alternatively, the quadrupole coupling can be formulated in terms of the component of largest magnitude, P_z^N, and the anisotropy parameter, $0 \leq \eta = (P_x^N - P_y^N)/P_z^N \leq 1$. Note that the goals of the present paper are adequately served by use of eq 2 and 3; more rigorous data analysis required for other purposes will be presented later.

The nuclear Larmor frequency normally is given by $\nu_N^\circ = g_N\beta_n H_0$ where g_N is the g factor for the free nucleus. However, the $m_s = \pm{}^3/_2$ electronic spin doublet that arises from the zero-field splitting of the total spin $S = {}^3/_2$ ground state of the MoFe protein (Figure 1 inset) provides a low-lying electronic state that gives rise to a large, anisotropic pseudo-nuclear Zeeman effect.[20a] This leads to an effective nuclear Larmor frequency, $\nu_N = g^N\beta_n H_0$, determined by the effective nuclear $\mathbf{g}^N$ tensor that is coaxial with the zero-field splitting tensor and has principal components[27]

$$g_\parallel^N = g_z^N = g_N$$

$$g_j^N = g_N\{1 + {}^3/_2(g\beta/g_N\beta_n)(A_j/\Delta)\} \quad j = x,y \tag{4}$$

In particular, the direction of $g_\parallel^N$ corresponds to that of the axial zero-field splitting component (D) and thus to the g_z axis of the electron Zeeman $\mathbf{g}'$ tensor. For nuclei with small g_N such as ^{57}Fe and ^{95,97}Mo the effect can be large and, depending on the magnitude of A_j^N/Δ and the sign of A_j^N, ν_N may range from $\nu_N \gg \nu_N^0$ through $\nu_N \sim 0$, and even $\nu_N < 0$, the latter corresponding merely to a reversal of the line positions.

The MoFe protein samples employed in this study are frozen solutions and thus contain centers having a distribution of orientations. Field positions at the extreme edges of the EPR spectrum, near either g_z' or g_y' (positions a and d in Figure 1) will give single-crystal-like ENDOR patterns associated with those molecules having a magnetic field directed along the corresponding $\mathbf{g}'$ tensor axes.[21,28] ENDOR signals at field b (Figure 1) will arise from molecules with H_0 along g_x', but to these will be added the signals from a well-defined subset of orientations for which the angle-dependent g value equals g_x'. ENDOR at any other intermediate field such as c similarly involves a well-defined subset of molecular orientations. ENDOR patterns obtained at fields away from the EPR spectrum edges are amenable to analysis through our theory of polycrystalline ENDOR spectra,[21] through consideration of spectra collected at many fields, the full nuclear hyperfine coupling tensor can be determined. Except where such an approach is necessary for the purposes of this paper, these analyses will be described at a latter date.

^{1}H ENDOR. Setting the magnetic field to the extreme high-field edge ($g_z' = 2.01$) of the ^{100}Mo-enriched Avl, Kpl, and Cpl EPR spectra yields the well-resolved single-crystal-like proton ENDOR spectra of Figure 2. From eq 2, the normal ENDOR pattern for a set of magnetically equivalent protons ($I = {}^1/_2$) is a pair of lines centered at the free-proton Larmor frequency, $\nu_H^\circ = g_H\beta_n H_0/h$ (14.62 MHz at 3200 G), and separated in frequency by the hyperfine coupling constant A^H ($\nu_\pm = \nu_H \pm A^H/2$). To achieve the illustrated high resolution and nearly equal intensity of a $\nu_\pm$ pair, it was necessary to take slow scans (0.1 MHz/s) and to accumulate for more than 3 h. At more rapid sweep rates (e.g., 0.375 MHz/s) the signal-to-noise ratio is considerably improved, but resolution is reduced and the spectra deviate appreciably from the ideal of symmetric intensity about ν_H (Figure 2).

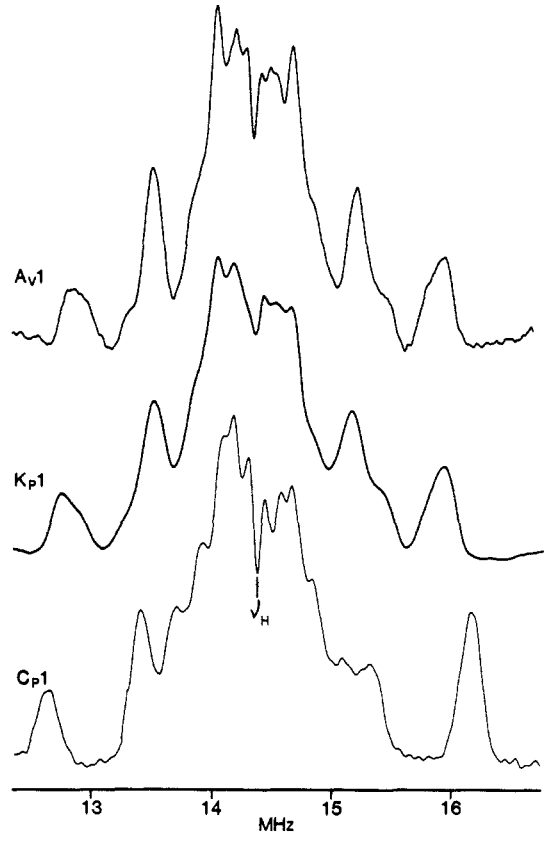

Figure 2. ^{1}H ENDOR spectrum at g_z' of the Avl, Kpl (pH 8.0), and Cpl (pH 8.6) MoFe proteins. Conditions: H_0 = 3360 (Avl), 3362 (Kpl), 3355 G (Cpl); T = 2 K; microwave power, 0.063 mW; 100-kHz field modulation, 1.25 G; rf power, 10 W; rf scan rates, 0.1 MHz/s (Avl, Cpl) and 0.375 MHz/s (Kpl).

Careful study of each of these ENDOR spectra shows the existence of numerous sets of magnetically equivalent protons, with coupling constants in the range of $0.14 < A^H < 3.6$ MHz (Table II). The overall pattern is similar in each case, but the spectra and coupling constants for Avl and Kpl are essentially the same, whereas those of Cpl differ somewhat. For example, the largest ^{1}H coupling of Cpl is greater than that for the other two proteins, and the Cpl resonances are better resolved (Table II). At least some of these doublets correspond to more than a single proton; this is obvious in the shapes of the peaks comprising the most strongly coupled doublet of Avl and Kpl and is more generally true because we find that perturbation of the protein by various agents can give rise to a partial loss of intensity of a doublet. Moreover, it is clear that the resolved features are riding on unresolved intensity from other protons. Much of this probably reflects a single broad underlying distant ENDOR peak, but some of the intensity may be associated with protons of the cluster. The observation of resonances from many protons is clearly consonant with the conclusion, obtained from analysis of the Mössbauer data,[10,11] that the paramagnetism of this center arises from spin coupling among a number of component metal atoms.

There has been essentially no information to date as to whether the cluster of the resting state (as isolated) enzyme exhibits sites that bind H_2O, OH^-, substrates, and/or inhibitors. In order to obtain evidence regarding such sites, we examined the proton ENDOR of samples subjected to D_2O exchange. When H_2O/D_2O comparisons were made it was impractical to use the slow-sweep conditions due to the long acquisition time required and the inadequate signal-to-noise ratio. However, more rapid sweeps, giving slightly lower resolution but better signal-to-noise, gave satisfactory results, and the comparisons were independent of the actual sweep rates employed.

(27) This expression ignores the rhombic splitting of the electron g tensor, which causes further rhombic splitting of the nuclear $g^{(n)}$ tensor; we have derived the general equation and find the correction to be unimportant.

(28) Rist, G. H.; Hyde, J. S. *J. Chem. Phys.* **1970**, *52*, 4633–4643.

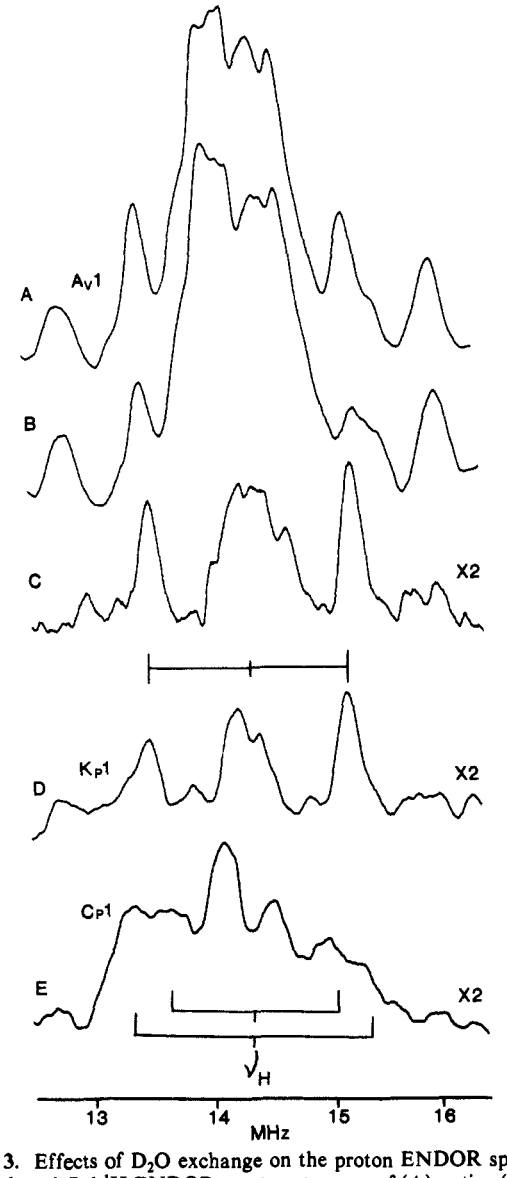

Figure 3. Effects of D_2O exchange on the proton ENDOR spectra of Avl, Kpl, and Cpl ^1H ENDOR spectra at $g = g_z$ of (A) native (pH 8.0) and (B) D_2O-exchanged Avl MoFe protein (pD 8.0). The digital subtraction (C) = (A) − (B) shows a strongly coupled exchangeable proton as well as a diminished distant ENDOR peak in the D_2O sample. The analogous digital subtraction (D) obtained for the Kpl protein is extremely similar. The digital subtraction (E) for Cpl exhibits two exchangeable doublets. Conditions: as in Figure 2, except that rf scan rates are 0.375 MHz/s.

When Avl is subjected to exhaustive D_2O exchange (Figure 3A–C), a single proton doublet with a 1.76-MHz coupling constant is significantly reduced in intensity. Thus, this resonance is associated with an exchangeable proton(s), possibly an H_2O or –OH group. An additional difference feature, centered at ν_H, also is seen upon D_2O exchange; this most probably represents a loss in intensity of the distant ENDOR from solvent. Resonances that persist could in part represent buried protons that are otherwise exchangeable (e.g., amide) but in the main are assignable to structural protons associated with hydrogens of amino acid residues that coordinate to the center and link it to the protein.

Figure 3 also shows the analogous digital subtractions of D_2O spectra from H_2O spectra for the MoFe proteins of Cpl and Kpl. The Kpl H_2O/D_2O difference (Figure 3D), although of poorer quality, is essentially the same as that for Avl, with a single exchangeable doublet, A^H = 1.67 MHz, and a central feature. The Cpl difference spectrum (Figure 3E) exhibits doublets from two exchangeable protons having coupling constants of 1.44 and 1.88 MHz. These two doublets have an average coupling (1.66 MHz) very similar to that of the single exchangeable proton

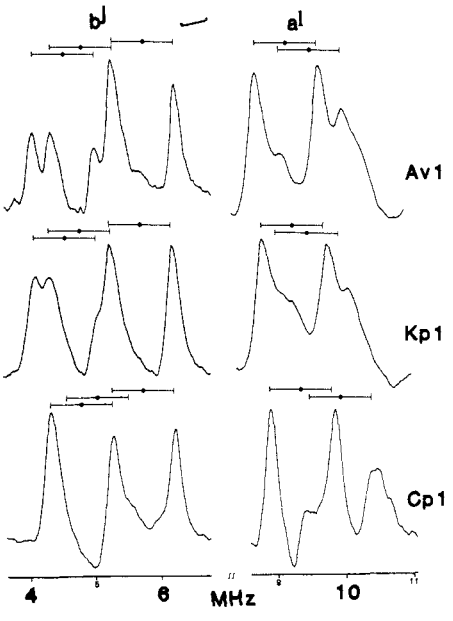

Figure 4. ^{57}Fe ENDOR of Avl, Kpl, and Cpl at g_z'. The assignment of five Larmor-split doublets is indicated, as are the frequencies corresponding to $A/2$ (●). Conditions: H_0 = 3360 (Avl), 3355 (Cpl), 3362 G (Kpl); T = 2 K; microwave power, 0.63 mW; 100-kHz field modulation, 4G; rf power, 30 W; rf scan rate, 3.5 MHz/s. The spectra were taken in segments, as indicated, with each segment representing ca. 2000 scans.

doublet of Avl (1.76 MHz) and identical with that of Kpl, suggesting that the associated atoms are, in all probability, chemically homologous. For example, the single exchangeable doublet seen for Avl and for Kpl could in each case represent two equivalent protons that become nonequivalent in the Cpl environment. An attractive chemical assignment of these resonances would be as the two protons of a water molecule associated with the cluster.

^{57}Fe ENDOR. High-Field Spectra. When the magnetic field is set to the extreme high-field edge of the EPR spectrum (field a, Figure 1B) of ^{57}Fe-enriched Avl, Kpl, or Cpl, single-crystal-like ENDOR spectra (Figure 4) are obtained. They arise from those molecules oriented such that the magnetic field lies along the g_z' axis of the g′ tensor. These resonances are not observed in unenriched samples and thus represent ^{57}Fe ENDOR from the cluster irons. Because of the superb resolution and excellent signal-to-noise, the peak positions have been measured with exceptionally high accuracy. Although this is not of major importance here, it will become so when we report the effects of substrates and inhibitors on these iron sites.

The ENDOR pattern of an individual ^{57}Fe nucleus ($I = 1/2$), or set of equivalent nuclei, consists of a pair of lines centered at $A'/2$ and split by $2\nu_{Fe}°$, $\nu_\pm = A'/2 \pm \nu_{Fe}$; for example, $2\nu_{Fe}°$ = 0.963 MHz at 3500 G. With the field along g_z, the pseudo-nuclear Zeeman effect is negligible (eq 4) and the ^{57}Fe ENDOR spectra of Avl and Kpl exhibit five resolved ^{57}Fe doublets split by $2\nu_{Fe}$, thereby directly demonstrating that the cluster comprises at least five distinguishable iron sites. The doublets form two groups (Figure 4), a lower frequency pattern centered at $A_z'/2 \sim$ 5–6 MHz consisting of a trio of resolved doublets and a group of lines centered at $A_z'/2 \sim$ 10 MHz consisting of at least two resolved doublets. In both proteins the apparently greater breadth of the highest frequency doublet suggests that it may arise from two very nearly equivalent sites. The assignment to sites labeled a^1, a^2, and b^1–b^3 is indicated in Figure 4, and the derived hyperfine couplings are given in Table II. The results for Avl differ slightly from the preliminary values reported earlier;[19] increased spectrometer sensitivity and stability have improved the resolution to the point where it is possible to reassess peak assignments and to measure the couplings to very high precision. In the Cpl spectra not all of the doublets are resolved (Figure 4); assignments of overlapping peaks have been made by analogy to the Avl and Kpl data. The value of A_z for each of the five iron sites of Cpl giving resolved

Table II. ^{1}H, ^{57}Fe, ^{95}Mo, and ^{33}S Hyperfine and Quadrupole Couplings (MHz) for Avl, Kpl, and Cpl Proteins in the $S = {}^{3}/_{2}$ Representation[a]

nucleus	protein	tensor projection	site[b] 1	2	3	4	5	6	7
^{1}H	Avl	$\|A_z\|$	3.16	2.20	1.76[c]	0.98	0.62	0.26	0.14
	Kpl		3.22	2.19	1.67[c]	1.34	0.62	0.35	0.16
	Cpl		3.60	1.88[c]	1.44[c]	0.92	0.56	0.34	0.14

nucleus	protein	tensor projection	site[b] a^1	a^2	b^1	b^2	b^3
^{57}Fe	Avl	$\|A_z\|$[d]	19.40	18.66	11.58	9.84	9.28
	Kpl		19.33	18.68	11.58	9.70	9.28
	Cpl		20.08	19.04	11.74	10.24	9.87

nucleus	protein	tensor projection	site[b] A^1	A^2	A^3[f]	B^1	B^2
^{57}Fe	Avl	A_y[d,e]	−20.60	−14.48	(−11.6)	+11.34	+8.86
			−20.66	−14.64		+11.42	+8.94
	Kpl		−20.57	−14.51	(−11.6)	+11.12	+8.74
			−20.77	−14.61		+11.28	+8.88
	Cpl		−21.22	−15.10	(−11.9)	+11.31	+9.18

nucleus	protein		hyperfine parameter
^{95}Mo	Kpl	$\|A_z^{Mo}\|$[g]	8.1
	Cpl		8.1
	Kpl	A_y^{Mo}[f]	+4.7
	Cpl		+5.4
	Kpl	$\|P_z^{Mo}\|$[h]	~1.6
	Cpl	η[h]	~1
^{37}S[i]	Cpl	A_z^S	−(<16)
		A_y^S	−(11–13)
		$\|P_y\|$	<1

[a] In some cases, couplings are indicated to be approximate or to cover a range of values. Uncertainties for specified couplings are as follows: or protons, ±1% for resolved resonances; for ^{95}Mo, ±0.2 MHz; for the ^{57}Fe resonance, ±0.01 MHz except for the A_y values for the site A^1, ± 0.02 MHz (see Experimental Procedures); the A^3 site is different (see text and below). [b] Many of these appear to represent at least two types of protons (see text). [c] Exchangeable, at least in part. [d] Correspondence between A_z and A_y values is not yet established, nor are the signs of A_z. For this reason the sites distinguished at g_z and g_y are labeled with lower and upper case letters. [e] Where two results are given, the upper was obtained with the field set to g_y', the lower with the field set 20 G below g_y'; for Cpl only g_y' was examined (see text). [f] Provisional assignments (see text); accuracy not adequate to warrant separate entries for the two field positions. [g] Hyperfine couplings have been calculated in a first-order fashion. [h] Values of P_z and η are indistinguishable for the two proteins. [i] Spectra at g_z demonstrate couplings to numerous sulfur sites; there is appreciable inequivalence, and it is not possible to assign individual hyperfine and quadrupole couplings. At g_y', all sulfurs appear to be roughly equivalent. Signs are provisional (see text).

resonances is essentially the same for the FeMo-co cluster of Avl and Kpl. However, the magnitude of the couplings is measurably greater for Cpl (Table II).

Low-Field Spectra. Single-crystal-like ^{57}Fe ENDOR spectra from the Avl, Kpl, and Cpl proteins also have been taken with the magnetic field set to the low-field edge of the EPR spectrum (position d of Figure 1B). For each of the three enzymes, data were taken with the magnetic field set to g_y', namely the low-field peak of the absorption derivative EPR spectrum (Figure 5). Six clearly articulated ^{57}Fe resonances, labeled 1–6, are observed in each case, with frequencies that range from ca. 9 to ca. 22 MHz. Signal strengths increase with frequency as expected;[20] the spectra shown were taken in segments as indicated, with each segment being normalized in intensity. As with the spectra of g_z', the sharp lines and the excellent signal-to-noise ratio permit us to measure peak positions with exceptional accuracy.

We have also explored in some detail the problem of obtaining authentic, limiting single-crystal-like spectra. In addition to the spectra in Figure 5, data for Avl and Kpl also were obtained by setting the magnetic field to the low-field half-height position of the g_y' peak in the absorption derivative EPR spectrum, 20 G below the field of g_y'. Although g_y' is associated with the flank of the absorption envelope, a field 20 G lower corresponds to the extreme edge of the spectrum where the intensity is only a few percent of that at the maximum of the absorption envelope. The coupling constants derived, as described below, from measurements at g_y' differ slightly from the limiting values obtained at the lower field; to illustrate this phenomenon, Table II presents both sets of values for Avl and Kpl. The lower field results were confirmed to represent true limiting values for the couplings by examining selected ^{57}Fe ENDOR peaks at a still lower field, 30 G below g_y'. The differences in Table II are not significant for present purposes but show that extreme care must be taken when making comparisons between data sets taken under different experimental conditions. This will be of importance when we discuss substrate binding.

Our preliminary report of ^{57}Fe ENDOR from the MoFe protein assigned each of the resonances seen at g_y' to a different type of iron site.[19] However, the availability of high-precision data from several enzymes in a variety of states has led us to reexamine and revise this assignment. A key outcome of this process has been the discovery that the ENDOR data can be used to calculate the signs as well as the magnitudes of the hyperfine coupling constants and also to provide high-precision values for the zero-field splitting parameter Δ.

With the field set to give a single-crystal-like ENDOR spectrum at g_y', each iron site is expected to give a Larmor doublet centered at $A_y'/2$. However, in contrast to spectra taken at g_z', the splitting by the effective nuclear Zeeman interaction at g_y' may be strongly affected by the pseudo-nuclear Zeeman effect (eq 4). For ^{57}Fe ($g_n = 0.18$) the nuclear Zeeman splitting may be written in mixed, but convenient units, as

$$2\nu_{Fe} = [1 + 1.02A\ (\text{MHz})/\Delta\ (\text{cm}^{-1})]2\nu_{Fe}^{\circ} \qquad (5)$$

where $2\nu_{Fe}^{\circ} = 0.433$ MHz at 1575 G. Using the reported value $\Delta \sim 10$ cm^{-1},[10] one obtains $2\nu_{Fe} = [1 + 0.1A\ (\text{MHz})]2\nu_{Fe}^{\circ}$. This equation predicts that the effective nuclear Zeeman splitting can differ drastically from the true nuclear Zeeman splitting, depending upon the sign and magnitude of A.

The measured separation of the g_y' Avl iron resonances labeled (1) and (2) (0.71 MHz) is in good agreement with the predicted splitting (eq 5) (0.82 MHz), taking the previously reported value of $\Delta \approx 12$ cm^{-1} and using the average frequency of peaks (1) and (2) to arrive at an $S = {}^{3}/_{2}$ representation hyperfine coupling

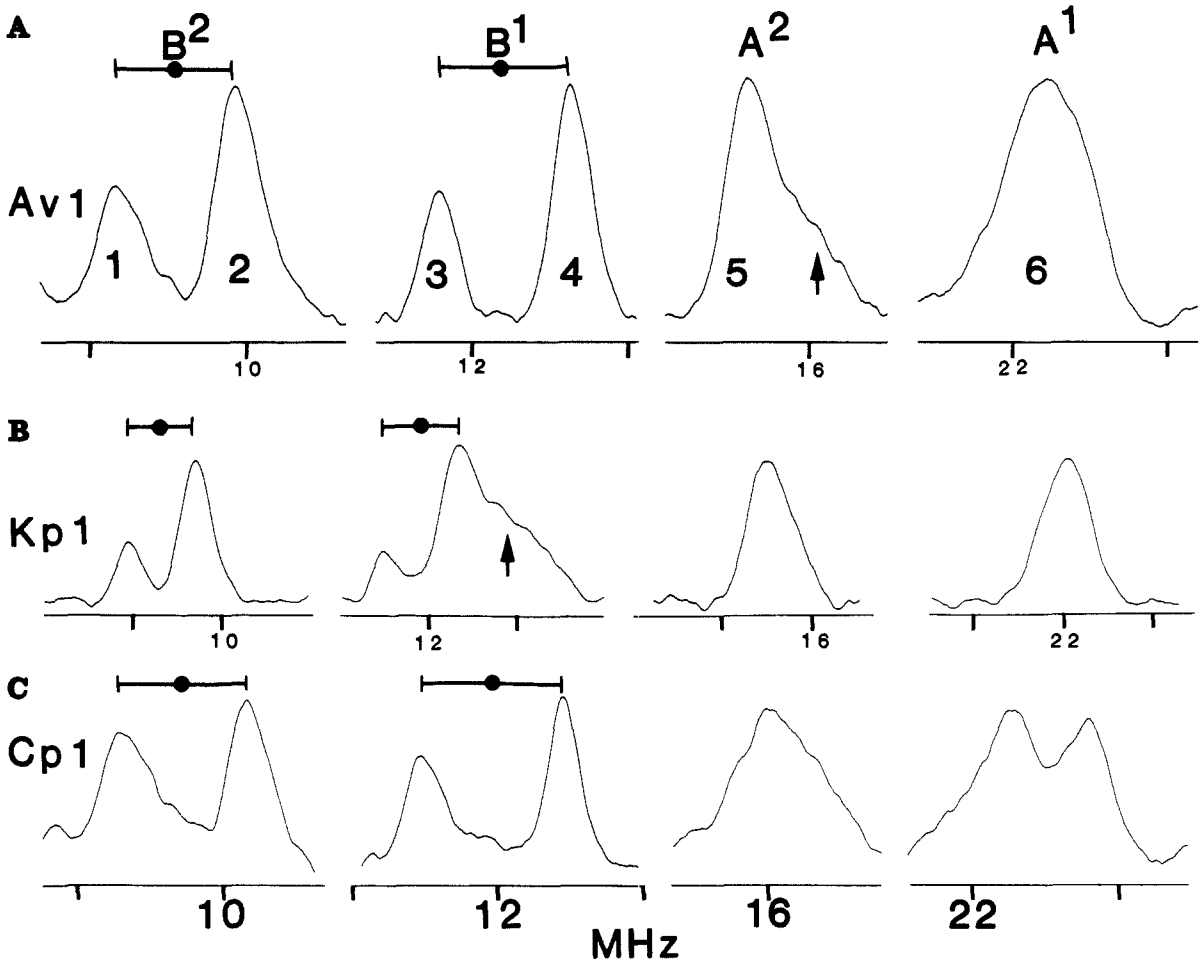

Figure 5. ^{57}Fe ENDOR of Avl, Kpl, and Cpl at g_y'. The peak numbering and assignments to individual sites are indicated; arrows denote shoulders that may represent resonances from other sites (see text). Conditions: H_0 = 1572 (Avl), 1570 (Kpl), 1578 G (Cpl); T = 2 K; microwave power, 0.63 mW; 100-kHz field modulation, 4G; rf power, 30 W; rf scan rate, 3.5 MHz/s. The ENDOR spectrum was taken in segments, as indicated, with each segment being normalized in height. Note that the scales differ. Each segment represents ca. 5000 scans.

constant (eq 3): A_y = +8.86 MHz. Best agreement with experiment is obtained by using Δ = 12.2 cm^{-1}. Equation 5 then becomes $2\nu_{Fe} = [1 + 0.08A\,(\text{MHz})]2\nu_{Fe}°$, which reproduces (0.76 MHz) the Fe(1)–Fe(2) splitting. In a similar fashion, if peaks (3) and (4) are taken to comprise a Larmor doublet from a site with coupling constant A_y = +11.34 for Δ = 12.2 cm^{-1}, the splitting, $2\nu_{Fe}$ = 0.83 MHz, is precisely reproduced by eq 4. Thus, we conclude that peaks (1) and (2) correspond to one iron site, labeled B^2 in Figure 5, and (3) and (4) to a second, labeled B^1, both having small, positive hyperfine couplings. The hyperfine coupling constants derived from these measurements are listed in Table II; the zero-field splitting parameters are listed in Table I. Note that the sites corresponding to the A_z couplings are labeled a^i and b^i in Table II to emphasize that no attempt is being made *in this paper* to correlate coupling constants measured at the high- and low-field edges of the EPR spectrum.

The ^{57}Fe ENDOR peaks (1)–(4) at g_y' for Cpl and Kpl have been analyzed in a fashion similar to that for Avl. The coupling constants for the B^1 and B^2 sites are similar to those for Avl and are listed in Table II; analysis of the nuclear Zeeman splittings through use of eq 4 gives the zero-field splittings in Table I. Finally, note that peak (4) is relatively symmetric for Avl and Cpl but shows a distinct high-frequency shoulder for Kpl. We return to this below.

The g_y' peaks (5) and (6) for Avl and Kpl are relatively broad singlets whose respective frequencies are the same for the two proteins. However, note again a high-frequency shoulder on peak (5) of Avl. The corresponding features for Cpl differ in frequency, and peak (6) for this protein is split, but by much less than $2\nu_{Fe}°$. In each protein the center frequency of peak (5) and of peak (6) can be interpreted in terms of an iron site whose hyperfine coupling constant is negative; in this case the direct and pseudo-nuclear Zeeman effects are opposed, and with the exception of peak (6) of Cpl, $2\nu_{Fe}$ becomes unresolvably small (eq 4). For example, from the frequency of Avl peak (5) one obtains a coupling constant, A_y = −14.48 MHz; taking Δ from Table I, eq 4 predicts a doublet splitting of −0.07 MHz. Similarly, resonance (6) of Avl corresponds to A_y = −20.60 MHz, giving $2\nu_{Fe}$ = −0.28 from eq 4. The small splittings calculated for peaks (5) and (6) of Kpl and for peak (5) of Cpl would not be resolved, and thus the assignment explains the ^{57}Fe ENDOR singlets. It also explains why peak (6) of Cpl is resolved into a doublet. Because Δ is slightly smaller for Cpl, the pseudo-nuclear Zeeman effect is larger and eq 4 predicts a resolvable splitting of $2\nu_{Fe}$ = −0.42 MHz, in satisfactory agreement with observation (magnitude 0.50 MHz). The hyperfine coupling constants for the iron sites associated with resonances (6) and (5) for three proteins are labeled A^1 and A^2 and are listed in Table II. Again, the Avl and Kpl couplings are similar, but those of Cpl are significantly greater in magnitude.

These assignments of the g_y' ^{57}Fe ENDOR spectra of the MoFe proteins have been confirmed by experiments performed on Avl and Kpl using several microwave frequencies. As the microwave frequency (ν_M) is varied, the magnetic field strength corresponding to a feature such as g_y' varies proportionately ($h\nu_M = g\beta H$) as does the nuclear Larmor splitting in an ENDOR spectrum associated with that feature. On the other hand, the hyperfine coupling constant is field independent, and the center frequency of a doublet should be independent of microwave frequency. As displayed in Figure 6, the splitting between resonances (1) and (2) increases as the microwave frequency increases (0.67 MHz at 8.69 GHz to 0.79 MHz at 9.95 GHZ), in good agreement with the predicted splittings using eq 4 (0.69 MHz at 8.69 GHz and

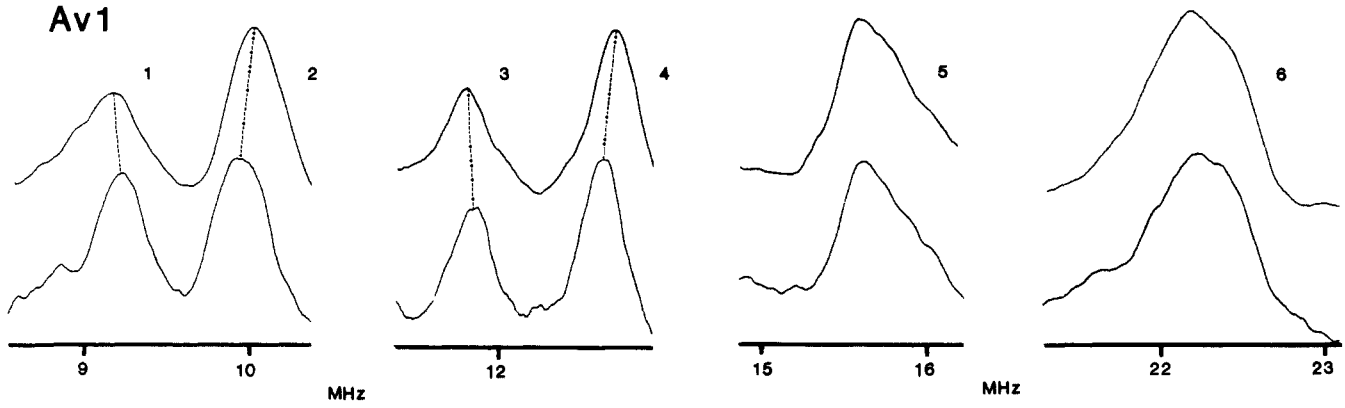

Figure 6. ^{57}Fe ENDOR of Avl (g_y') at two different microwave frequencies: upper, 9.95 GHz (H_0 = 1645); lower, 8.69 GHz (H_0 = 1436). Note that peaks (5) and (6) are invariant with microwave frequency, but the (1)–(2) and (3)–(4) frequency differences increase at the higher microwave frequency. Conditions are the same as for Figure 5. The spectrum was taken in segments, as indicated, with each segment being normalized in height.

0.79 MHz at 9.95 GHz). The same effect is observed for resonances (3) and (4), the splittings increasing from 0.74 MHz at 8.69 GHz (0.77 MHz predicted) to 0.84 MHz at 9.95 MHz (0.88 MHz predicted). As expected, resonances (5) and (6) remain stationary, their splittings still unresolvable (predicted: peak (5), −0.08 MHz at 8.69 GHz and −0.10 MHz at 9.95 GHz; peak (6), −0.29 MHz at 8.69 GHz and −0.33 MHz at 9.95 GHz). These results fully confirm assignment of resonances (1)–(4) as representing two sites, B^2 and B^1.

Although the g_z' ^{57}Fe ENDOR spectra of Avl and Kpl contain resolved resonances from five iron sites and are suggestive of a sixth (Figure 4), the g_y' spectra of Avl and Cpl (Figure 5A,C) contain resolved resonances from only four iron sites, A^1, A^2, B^1, and B^2. However, as noted above, peak (4) of Kpl and (5) of Avl each has a distinct high-frequency shoulder. Simulations of polycrystalline ENDOR spectra[21] indicate that such features should not occur in a single-crystal-like ENDOR spectrum from a single, homogeneous, and distinct site. Considering the overall similarity between Avl and Kpl and even Cpl, this raises the possibility that, in all three proteins, peaks (4) and/or (5) represent overlapping resonances from two distinct sites.[29] This issue is being addressed through a detailed analysis of spectra that have been taken across the entire envelope of the EPR spectrum and will be reported later. The results to date indicate that peak (5) represents a single type of iron site but lead us to assign peak (4) as being a superposition of the high-frequency partner of the site B^1 Larmor doublet and of a single peak corresponding to an additional site, A^3, having the negative hyperfine coupling listed in Table II. From eq 4, such a coupling would give $2\nu_{Fe} \sim 0$ and a single peak.

The current state of the analysis further shows that the differences among the iron sites disclosed in the single-crystal-like spectra are not simply interpretable in terms of equivalent iron sites that have different orientations with respect to the g tensor coordinate frame: Each of the magnetically distinct sites detected by ENDOR measurements indeed appears to have distinct hyperfine tensor principal values, and thus distinguishable chemical characteristics.

^{95,97}Mo ENDOR. We have examined the ENDOR spectra of ^{95}Mo- ($I = {}^5/_2$) and ^{97}Mo- ($I = {}^5/_2$) enriched Cpl and of ^{95}Mo-enriched Kpl. In order to characterize the molybdenum site, it proved necessary to collect single-crystal-like ENDOR spectra at both the high-field (g_z', Figure 1B, a) and low-field (g_y', Figure 1B, d) edges of the EPR envelope and at numerous intermediate field strengths (e.g., Figure 1B, b and c). Figure 7 presents the ENDOR patterns obtained at the high-field edge by computer

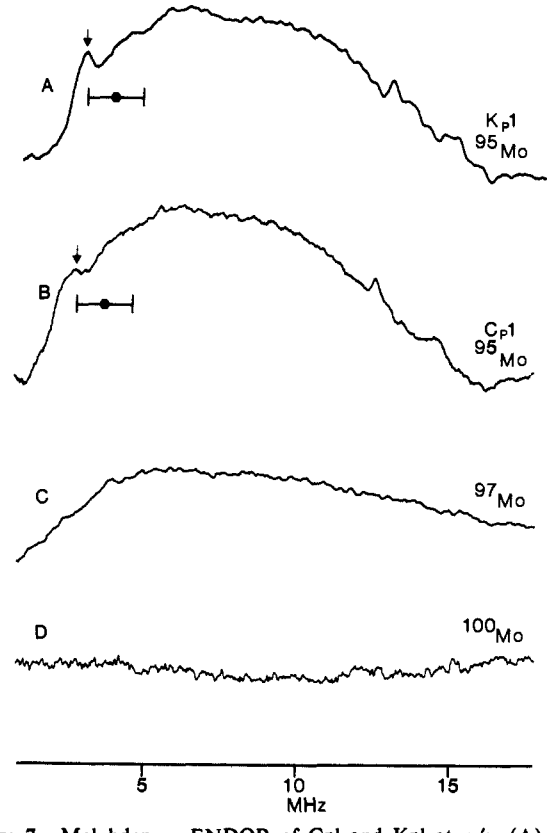

Figure 7. Molybdenum ENDOR of Cpl and Kpl at g_z': (A) ^{95}Mo ENDOR of Kpl obtained by subtracting the spectrum of a ^{100}Mo-enriched sample from that of a ^{95}Mo-enriched sample; (B) ^{95}Mo ENDOR of Cpl obtained by a subtraction procedure analogous to that in A (the features indicated by the arrow in A and B are discussed in the text); (C) ^{97}Mo ENDOR of Cpl obtained from ^{97}Mo- and ^{100}Mo-enriched samples by subtraction; (D) digital subtraction of two separate ^{100}Mo spectra. Conditions: H_0 = 3350 (Cpl), 3360 G(Kpl); T = 2 K; microwave power, 0.2 mW; 100-kHz field modulation, 4 G; rf power, 30 W; rf scan rate, 2.5 MHz/s.

subtracting an ENDOR trace of a ^{100}Mo- ($I = 0$) enriched protein from that of the corresponding protein grown with Mo of nonzero nuclear spin. The ^{95}Mo signals from the two proteins span the frequency range from roughly 0 to ca. 15 MHz. The trace from ^{97}Mo-enriched Cpl is weaker and broader to the point that it is not possible to determine where the trace returns to base line at high frequencies. The following observations identify these signals with molybdenum ENDOR transitions: (1) Subtractions involving numerous independently collected spectra of ^{95}Mo-enriched and ^{100}Mo-enriched Cpl and Kpl samples yield the same feature. (2) Subtractions of independent spectra from a ^{100}Mo-enriched sample taken on separate days are featureless (Figure 7D), demonstrating

(29) We also note that in endor spectra at g_y' there are proton resonances near the proton Larmor frequency (~7 MHz) in the natural-abundance protein whose absence in the spectrum from a ^{57}Fe-enriched sample might indicate that the proton resonances overlap and cross relax an additional iron resonance, making both resonances unobservable. This possibility will be checked with measurements at a higher spectrometer frequency.

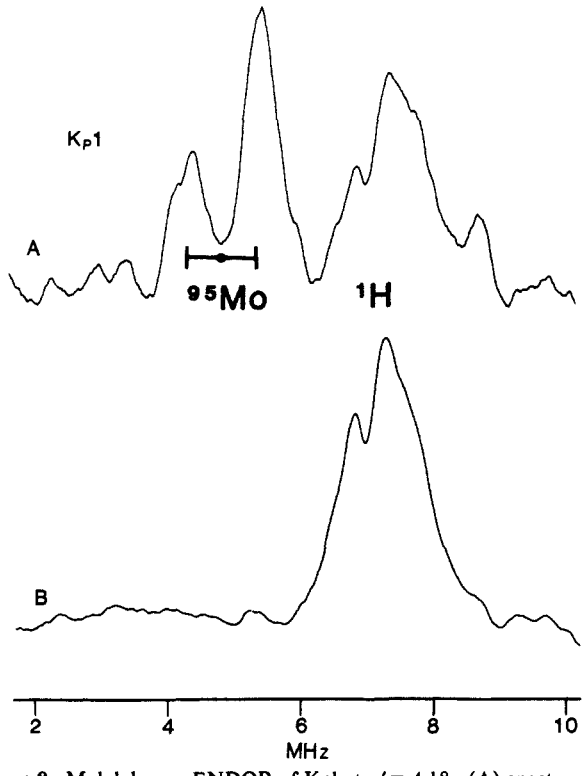

Figure 8. Molybdenum ENDOR of Kpl at $g' = 4.18$: (A) spectrum of ^{95}Mo-enriched sample; (B) spectrum of ^{100}Mo-enriched sample. Conditions: $H_0 = 1625$ G; $T = 2$ K; microwave power, 0.2 mW; 100-kHz field modulation, 4 G; rf power, 30 W; rf scan rate, 2.5 MHz/s.

that the subtraction technique effectively eliminates consistent base-line shifts.

The ^{95}Mo spectra of Cpl and Kpl at g_z' are qualitatively similar to that reported earlier for Cpl.[18] However, the improved signal-to-noise in these spectra has revealed that the pattern is broader than previously observed. It also permits identification of a shoulder at ~3.2 MHz on the low-frequency edge of the Cpl ^{95}Mo spectrum and of a corresponding resolved peak for Kpl. The weak, sharp features in the vicinity of ν_H (~13 MHz) are not significant, however; they are imperfectly cancelled proton resonances.

The ^{95}Mo spectra taken at fields near the low-field, g_y', edge of the EPR envelopes for Cpl and Kpl are dramatically different from the broad resonances at g_z'; comparison of such traces from ^{100}Mo- and ^{95}Mo-enriched Kpl (Figure 8) and Cpl shows that ^{95}Mo contributes a pair of sharp, well-resolved ^{95}Mo resonance, rather than the broad feature of Figure 7. In contrast, ENDOR spectra from the ^{97}Mo-enriched sample of Cpl give no evidence of intensity associated with ^{97}Mo ENDOR. If the ^{95}Mo peaks for Cpl and Kpl at g_y' are treated as a Larmor-split doublet centered at $A_y'^{Mo}/2$ according to eq 2, one obtains the values of A_y^{Mo} given in Table II. Note that this result once again discloses differences between Cpl and Kpl.

The assignment of the ^{95}Mo resonances is confirmed by considering the doublet splittings. For ^{95}Mo ($g_n = 0.36$), eq 4 predicts a Larmor splitting of

$$2\nu_{Mo} = [1 + 0.5A\ (\text{MHz})/\Delta\ (\text{cm}^{-1})]2\nu_{Mo}^{\circ}$$

where $2\nu_{Mo}^{\circ} = 0.874$ MHz at 1575 G. Taking A^{Mo} to be positive (Table II) and employing the values of Δ given in Table I, one obtains $2\nu_{Mo} = 1.10$ MHz for Cpl and 1.03 MHz for Kpl, in agreement with the measured values of 1.15 MHz for Cpl and 1.07 MHz for Kpl.

The g_y' ^{95}Mo ENDOR spectrum thus has the appearance expected for a nucleus of $I = {}^1/_2$, with no hint of the quadrupolar splittings predicted by eq 2, whereas the g_z' pattern is broad, presumably because of such splittings. In order to resolve this apparent contradiction, spectra were taken at fields across the envelope of the EPR spectrum of the two ^{95}Mo-enriched proteins; the results were similar, and those for Cpl are presented in Figure

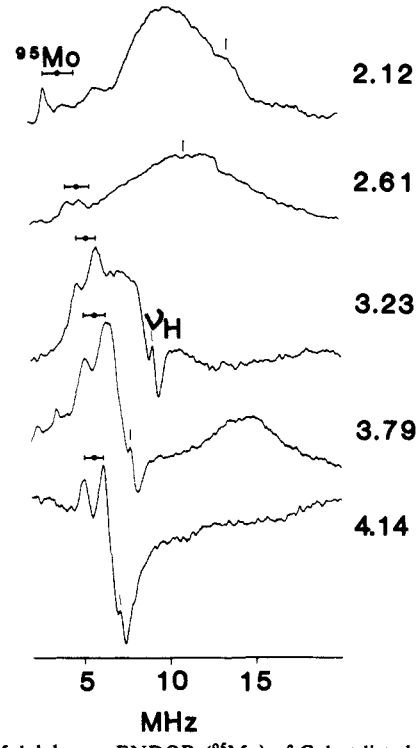

Figure 9. Molybdenum ENDOR (^{95}Mo) of Cpl at listed g values corresponding to fields across the EPR absorption envelope. Traces represent the subtraction [^{95}Mo − ^{100}Mo]. The center (·) and splitting (|—|) of the ^{95}Mo m_I ($\pm{}^1/_2$) Larmor doublet is indicated in each spectrum; a vertical line corresponding to ν_H also is included. Note the negative-going features at $g \geq 3.23$, which correspond to proton resonances that are partially suppressed in the ^{95}Mo sample. Conditions: $T = 2$ K; microwave frequency, 9.502 GHz; microwave power, 0.2 mW; 100-KHz field modulation, 4 G; rf power, 30 W; rf scan rate, 2.5 MHz/s.

9 in the form of [^{95}Mo − ^{100}Mo] subtractions. As the field is decreased from g_z', the low-frequency shoulder on the Cpl ^{95}Mo ENDOR trace becomes more pronounced and better resolved and is seen to be the lower frequency partner of a Larmor-split doublet such as seen in Figure 8. As this occurs, the broad, main feature at g_z' broadens further, weakens, and is eventually lost. In contrast, ^{97}Mo resonances were not detected at any field appreciably below the high-field edge of the EPR spectrum.

The combined observations of molybdenum ENDOR can be explained as follows: The sharp ^{95}Mo features indicated in Figures 7–9 correspond to the Larmor doublet associated with the $m_I = +{}^1/_2 \leftrightarrow -{}^1/_2$ nuclear transitions described by eq 2. The shift in frequency of these transitions with observing field is caused by anisotropy of the A′ tensor; use of eq 3 indicates a real anisotropy of the ^{95}Mo coupling in the $S = {}^3/_2$ representation (Table II). The broad feature that appears most prominantly at g_z' (Figure 7) and that alters and vanishes at lower fields (Figure 9) arises from the other so-called "satellite" transitions[30] within the $I = {}^5/_2$ nuclear spin manifold of states.

The breadth of the ^{95}Mo pattern at g_z' is determined by the satellite transitions and for both Cpl and Kpl can be given a first-order discussion (eq 2) if we use $\nu_n^{\circ} = 0.9$ MHz, A^{Mo} as given in Table II, and $P_z \approx 1.6$ MHz. Of course, when the quadrupole coupling is not small compared to the hyperfine interaction, a first-order treatment is adequate for the qualitative discussion presented here but is not quantitatively reliable. The featurelessness of the g_z' resonances (Figure 7) further suggests a distribution in the quadrupole coupling parameter and/or in the relative orientation of the quadrupole splitting tensor.

Why do the satellite transitions vanish at low observing fields? The frequencies of the satellite transitions, but not the m_I ($\pm{}^1/_2$) doublet, depend strongly on the principal quadrupole splitting, P_z^{Mo}, the asymmetry, $\eta = (P_x^{Mo} - P_y^{Mo})/P_z^{Mo}$, and the orientation of the field with respect to the tensor axes (eq 2).[20a] Simulations of ^{95}Mo ENDOR patterns indicate that the field dependences of Figures 7–9 are associated with a quadrupole tensor that has P_z

$\approx$ 1.6 MHz and maximal rhombicity: $\eta \sim 1$ ($P_y \sim 0$; $P_x \sim -P_z$). In that case the quadrupole splittings are predicted to vanish when the field lies near g_y', as observed. At intermediate field values the ENDOR signal arises from centers having a range of orientations with respect to the field, and the simulations show that the quadrupole interactions cause the satellite transitions to spread over a broad frequency range. For observing fields corresponding to $g' \lesssim g_x'$, the predicted intensity of these transitions is substantial, but for $g' \gtrsim g_x'$, their intensity is greatly reduced compared to the m_I ($\pm^1/_2$) doublet. Moreover, we noted above that the ^{95}Mo spectrum at g_z' gives evidence that the quadrupole parameters exhibit some distribution in values. This distribution would compound the spread of the satellite transitions without affecting the m_I ($\pm^1/_2$) doublet. This would further reduce the intensity of the former, which explains their indetectability at low observing fields. An analogous situation arises in nuclear magnetic resonance spectroscopy of quadrupolar nuclei; when quadrupole couplings are large and nonaxial, the satellite lines can be undetectably broad even though the m_I ($\pm^1/_2$) lines remain observable.[30]

This interpretation of the ^{95}Mo results is given independent support by the observations made with the ^{97}Mo-enriched complex. The quadrupole moment of ^{97}Mo is $\sim$10 times larger than that for ^{95}Mo,[31] and the ^{97}Mo quadrupole couplings are larger by the same ratio. This difference first of all explains the extreme breadth of the ^{97}Mo pattern at g_z' (Figure 7). Moreover, with such a large coupling, the m_I ($\pm^1/_2$) resonances would not remain even approximately independent of the quadrupole parameters, and a distribution in these parameters could render even the central doublet undetectable.

The small value of the ^{95}Mo hyperfine coupling suggests that the molybdenum is to be classified as a diamagnetic, even-electron ion with an even formal valency, and not as Mo(V) or Mo(III). Model studies show that hyperfine couplings for an isolated, sulfur-coordinated $S = {}^1/_2$ Mo(V) would be ca. 150 MHz[32] and that coupling constants for $S = {}^3/_2$ Mo(III) would be comparable.[33] This is roughly 20-fold larger than we observed, and thus an isolated Mo ion having either of these two formal valences would not be acceptable, the former case doubly so because it has the wrong spin. If the $S = {}^3/_2$ ground state of FeMo-co were achieved by spin coupling between an $S = {}^1/_2$ Mo(V) and the net spin of the six iron atoms, the intrinsic molybdenum hyperfine coupling would be strongly reduced.[18] The reduction would be maximal (5-fold) if the resultant $S = {}^3/_2$ state of the center were achieved by antiferromagnetic coupling of the $S = {}^1/_2$ molybdenum with a net iron spin of $S = 2$, but this model still would predict a hyperfine interaction of $\sim$30 MHz, no less than ca. 4-fold larger than observed. Spin coupling between an $S = {}^3/_2$ Mo(III) and the net iron spin is even less favorable; an $S = {}^3/_2$ molybdenum and a net $S = 3$ iron spin would reduce the ^{95}Mo hyperfine interaction of an isolated molybdenum by only 40%, to $\sim$90 MHz. These coupling schemes are highly simplified, and it is quite possible that spin coupling within the cluster could fortuitously lead to a small ^{95}Mo coupling. Just such a situation occurs for one of three iron sites within an [3Fe–3S] cluster.[34] However, the simplest assignment, to a nonmagnetic molybdenum valency, certainly seems preferable at this stage. Combined with the X-ray absorption edge study[17] favoring Mo(III) or Mo(IV), the hyperfine couplings suggest an assignment of Mo(IV).

Further insights into the state of the molybdenum can be achieved by considering the ^{95}Mo quadrupole coupling parameters inferred from the ENDOR measurements. The quadrupole interaction strength, P_z, reflects the asymmetric distribution of electrons in the vicinity of the Mo nucleus. For a transition ion one expects, as a first approximation, that the quadrupole coupling will be determined by the imbalance in the d-orbital population. For example, the d-electron contribution to P_z^{Mo} is proportional to the total orbital populations of d_{z^2}, d_{xz}, and d_{yz} minus the populations of d_{xy} and $d_{x^2-y^2}$.[35] Thus, Mo(VI), d^0, would be expected to have a small quadrupole coupling compared to pseudooctahedral Mo(IV), d^2, which would have a net imbalance of two d electrons. However, asymmetric coordination to the metal can have a major influence on the quadrupole coupling, so it is necessary to compare the quadrupole interaction of ^{95}Mo in the cofactor cluster of the MoFe protein with those of molybdenum in Mo^{IV} and Mo^{VI} complexes of well-defined Mo valency and coordination environment. A preliminary comparison recently has become possible through progress in ^{95}Mo NMR measurements.

The ^{95}Mo NMR line widths of a diamagnetic Mo complex in solution are determined by nuclear quadrupole relaxation, and Enemark and his co-workers have shown that there is an intrinsic line width associated with a particular molybdenum coordination environment.[31] In this case the quadrupole coupling parameters can be obtained from the NMR line width, W (Hz), and the correlation time for molecular reorientation, τ_c. The well-known equation for quadrupolar relaxation[30c] can be rewritten[36]

$$P_z^{Mo}\,(\text{MHz}) = {}^1/_{24}\left(\frac{5}{\pi}\right)^{1/2}\left(\frac{W\,(\text{Hz})}{\tau\,(\text{ps})}\right)^{1/2}\left(1+\frac{\eta^2}{3}\right)^{-1/2} \qquad (6)$$

Since the asymmetry term must fall in the range $1 \leq (1 + \eta^2/_3)^{1/2} \leq 1.15$, it can be set to unity for present purposes.

Numerous mononuclear Mo^{VI} complexes have been studied by ^{95}Mo NMR,[31] and recently a number of Mo^{IV} complexes also have been examined.[37] Although the line width of Mo^{IV} and Mo^{VI} complexes do show an overlap in their ranges, as expected from the considerations of *d*-orbital occupancy, the Mo^{IV} complexes of well-defined covalency *typically* exhibit quadrupolar line widths, $W > 10^3$ Hz, that are large compared to those of Mo^{VI} complexes, for which $W \lesssim 10^2$ Hz is common. EXAFS measurements on nitrogenase[16,17] indicate that Mo is coordinated by four to five sulfurs and probably two oxygens (or nitrogens). At this time the mononuclear complexes studied by ^{95}Mo NMR that most nearly model this situation are sulfur-coordinated ($Mo^{IV}O$) species, for example, $[MoO(S_2CNEt_2)_2]$ whose ^{95}Mo quadrupolar line width is $W = 2700$ Hz, and analogous ($Mo^{VI}O$) and ($Mo^{VI}S_2$) complexes, for example, $[MoO(S_2CNEt_2)_3]^+$ ($W = 40$ Hz) and $[MoS_2(ONC_5H_{10})_2]$ ($W = 70$ Hz). In the absence of experimentally determined rotational correlation times, we can estimate τ_c for these complexes to be in the range $\tau_c \sim 15$–50 ps.[36] In this case, $W \sim (1-4) \times 10^3$ Hz for a $^{95}Mo^{IV}$ complex corresponds to $P_z^{Mo} \sim 1$ MHz, whereas $^{95}Mo^{VI}$ line widths of ca. 10^2 Hz would correspond to $P_z^{Mo} < 0.1$ MHz. Considering that $P_z^{Mo} \sim 1.6$ MHz for nitrogenase, this comparison would support an assignment of Mo^{IV} rather than Mo^{VI} for the MoFe protein. This assignment again is in consonance with Mo X-ray absorption edge measurements.[16c] The rhombicity of the ^{95}Mo quadrupole coupling further suggests a highly unsymmetric coordination environment of molybdenum in the cofactor cluster.

More extensive NMR studies will be necessary to confirm this conclusion. First of all, accurate NMR measurements of quadrupole parameters will require the use of τ_c that are experimentally determined. Of more fundamental importance, the NMR data show that the Mo coordination environment also can have a strong

(30) (a) Cohen, M. H.; Reif, F. *Solid State Physics*; Academic: New York, 1957; Vol. 5. (b) Das, T. P.; Hahn, E. *Solid State Physics*; Academic: New York, 1958; Suppl. 1. (c) Abragam, A. *Nuclear Magnetism*; Oxford University Press: Oxford, 1960.

(31) Minelli, M.; Enemark, J. H.; Brownlee, R. T. C.; O'Connor, M. J.; Wedd, A. G. *Coord. Chem. Rev.* **1985**, *68*, 169–278.

(32) Hanson, G. R.; Brunelle, A. A.; McDonnell, A. C.; Murray, K. S.; and Wedd, A. G. *J. Am. Chem. Soc.* **1981**, *103*, 1953–1964.

(33) Averill, B. A.; Orme-Johnson, W. H. *Inorg. Chem.* **1980**, *19*, 1702–1705.

(34) Emptage, M. H.; Kent, T. A.; Huynh, B. H.; Rawlings, J.; Orme-Johnson, W. H.; Münck, E. *J. Biol. Chem.* **1980**, *255*, 1793–1796.

(35) Lucken, E. A. C. In *Nuclear Quadrupole Coupling Constants*; Academic: New York, 1969.

(36) Equation 6 follows from eq 137, Chapter VIII, of Abragam (ref 30c) for $I = {}^5/_2$ when the line width is governed by quadrupolar broadening; P_z is defined subsequent to eq 3, above. The correlation time can be approximated from the expression for a spherical solute of radius a, $t_c = 4\pi\eta a^3/3kT$, using $Mo(CO)_6$ as a reference ($\tau_c^\circ = 8.5 \times 10^{-12}$ s in $CDCl_3$, a $\sim$ 3.5 Å) and an estimated radius for the molecule of interest as $\tau_c/\tau_c^\circ = (a/a_0)^3[\eta/\eta(CDCl_3)]$.

(37) Young, C. G.; Enemark, J. H. *Inorg. Chem.* **1985**, *24*, 4416–4419.

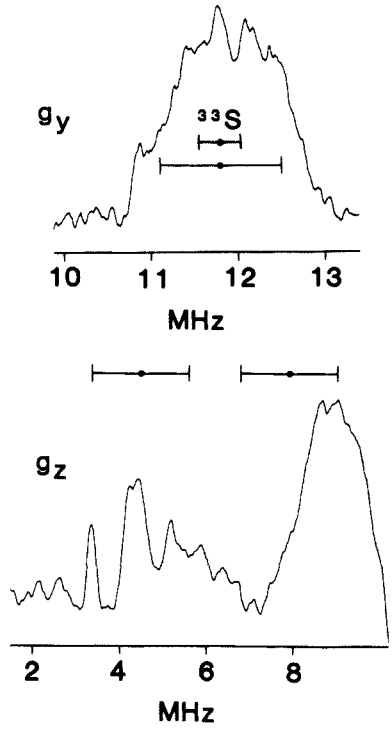

Figure 10. ^{33}S ENDOR spectrum of Cpl: upper, g_y' (H_0 = 1575 G), $A^S/2$ is indicated; lower, g_z' (H_0 = 3355 G). The nuclear Larmor splitting is indicated to help in assessing the many resonances. Conditions: T = 2 K; microwave power, 0.2 mW; 100-kHz field modulation, 2 G; rf power, 30 W; rf scan rate 10 MHz/s.

effect on the quadrupole couplings and suggest that discrimination between Mo^{IV} and Mo^{VI} on this basis in the unsymmetrical coordination environments considered here is meaningful, but by no means is without exceptions. Thus, systematic extension of current ^{95}Mo NMR studies using a wide range of coordination environments, as well as ENDOR on (Mo, Fe) clusters,[38] will play an important role in further clarifying the state of Mo in the MoFe protein.

^{33}S ENDOR. Setting the magnetic field to correspond to the low-field edge (g_y') of the EPR spectrum of a ^{33}S-enriched MoFe protein of Cpl yields a feature that is not present in the natural-abundance protein [Figure 10 (top)], and that represents the first reported ^{33}S ENDOR spectrum. Although no other ^{33}S resonances were observed, the signal is sufficiently weak that we cannot rule out the possibility that some features at frequencies below ~10 MHz were obscured by the proton signals or that a very anisotropic signal was too weak to detect. Considering that FeMo-co contains 9 ± 1 S^{2-}, the pattern of a single feature with barely resolved structure is surprisingly simple. The resonance presumably corresponds to a number of similar sulfur sites, and it appears that these must primarily, if not exclusively, correspond to the S^{2-} ions that bridge the metal sites of the cluster. The primary sequence of the MoFe protein shows no more than 16 conserved cysteines per molecule,[3a] and if there are four cysteinyl ligands per [4Fe–4S] P cluster center, then no mercaptides would be available for coordination to the FeMo-co. The recent observation of nitrogen coordination to the [2Fe–2S] Rieske-type center[39] does raise the possibility that the unusual properties of the P clusters may arise in some part from coordination by protein residues other than cysteine, thus leaving unaccounted conserved cysteines. Even if this is so, studies of the isolated cofactor[40] indicate that it cannot bind more than a single mercaptide.

^{33}S has a nuclear spin $I = {}^3/_2$, and each magnetically distinct site will give a pattern that is centered at $A^{S'}/2$ and can contain as many as four resolved lines (eq 2). From the center frequency of the pattern in Figure 10A and eq 2, $|A_y^S| \simeq 11.8$ MHz. Taking into account the pseudo-nuclear Zeeman effect, eq 3, the Larmor splitting is $2\nu_S = [1 + 0.043\ A^S\ (MHz)]2\nu_S°$, where $2\nu_S° = 1.0$ MHz at 1575 G. Taking A_y^S to be positive predicts $2\nu_S \sim 1.5$ MHz, which is nearly the full breadth of the ^{33}S ENDOR pattern (Figure 10, top). It seems reasonable instead to infer that A^S is negative, giving $2\nu_S \simeq 0.5$ MHz. The partially resolved structure probably reflects small quadrupole couplings and inequivalences among the contributing sulfur sites. It seems plausible that S^{2-} ions would acquire negative spin density through spin polarization and would largely be equivalent as suggested by the spectrum. Furthermore, small quadrupole couplings are suggestive of a closed-shell ion whose symmetric charge distribution is not highly distorted by the covalent bonding in the cluster.

The ^{33}S ENDOR spectrum of Figure 10 (bottom) is obtained when the magnetic field is set to the high-field, g_z', edge of the EPR spectrum; no other sulfur resonances are detected at higher frequencies. The complexity of this pattern indicates that the sites that appear to be equivalent at g_y' in fact have inequivalent degrees of hyperfine and/or quadrupole coupling anisotropy. It confirms that numerous sulfur atoms are magnetically coupled to the $S = {}^3/_2$ spin system but precludes an unambiguous analysis in detail. However, the mere fact that the resonances occur in the frequency range $\nu \lesssim 10$ MHz, with major intensity centered at ca. 5–6 MHz, indicates that the couplings for the different sites have values of A_z^S in the range 10–15 MHz and that none are substantially larger than A_y^S. In short, the ^{33}S couplings are roughly isotropic or, if anisotropic, are smaller than in an alkyl sulfur radical, RS·,[41] for which A^S is highly anisotropic and can range up to 160 MHz. Again, this is consistent with assignment of the ^{33}S resonances to S^{2-} ions.

Discussion

The ENDOR measurements described here have allowed us to compare at a microscopic level the catalytically active center of MoFe proteins isolated from three different organisms. We have observed six of the metal sites comprising the FeMo-co cluster in these proteins and structural *and* exchangeable protons associated with the cluster and have taken a first step in characterizing the sulfur atoms that link the metals and that attach the cluster to the protein. The results give a clear picture of the $S = {}^3/_2$ FeMo-co cluster as a complex, multimetal cluster whose properties are largely invariant to the origin of the protein environment. However, a subtheme that also emerges is that differences in the protein environment can produce pervasive, small differences throughout the structure: Avl and Kpl show consistent similarities in all properties, whereas Cpl is distinctly different in all measurements performed. The ENDOR spectroscopic characterization of these three MoFe enzymes thus gives a consistent microscopic correlate for known differences in catalytic properties: Avl and Kpl are quite similar with respect to cross-reaction with Fe proteins of different species[42] and the efficiency of N_2-dependent H/D exchange[43] and differ from Cpl.

All three proteins show ^1H resonances from numerous protons, consistent with the requirement that a multimetal cluster be attached to the protein by a number of amino acid residues. The coupling constants for Avl and Kpl are essentially identical, whereas Cpl exhibits distinct differences. No previous measurements have given direct evidence regarding sites on the resting-state cluster that coordinate small molecules. The observation by ENDOR of exchangeable proton resonances strongly suggests the presence of H_2O or OH^- bound to the cluster in that state. Avl and Kpl are again similar, showing a single exchangeable resonance, whereas Cpl shows two resonances whose

(38) (a) Holm, R. H. *Chem. Soc. Rev.* **1981**, *10*, 455–490. (b) Coucouvanis, D. *Acc. Chem. Res.* **1981**, *14*, 201–209.
(39) (a) Fee, J. A.; Findling, K. L.; Yoshida, T.; Hille, R.; Tarr, G. D.; Hearshen, D. O.; Dunham, W. R.; Day, E.; Kent, T. A.; Münck, E. *J. Biol. Chem.* **1984**, *259*, 124–133. (b) Cline, J. F.; Hoffman, B. M.; Mims, W. B.; La Haie, E.; Ballou, D. P.; Fee, J. A. *J. Biol. Chem.* **1985**, *260*, 3251–3254.
(40) Mascharak, P. K.; Smith, M. C.; Barmstron, W. H.; Burgess, B. K.; Holm, R. H. *Proc. Natl. Acad. Sci. U.S.A.* **1982**, *70*, 7056–7060.
(41) Gordy, W. *Theory and Applications of Electron Spin Resonance*; Wiley: New York, 1980.
(42) Emerich, D. W.; Burris, R. H. *J. Bacteriol.* **1978**, *134*, 936–943.
(43) Davis, L. C.; Wang, Y.-L. *J. Bacteriol.* **1980**, *141*, 1230–1238.

average coupling matches that for the other proteins.

Mössbauer spectra of the MoFe proteins have been interpreted in terms of isotropic hyperfine interactions with six cluster iron centers, three of which were treated as equivalent.[10,11] The single-crystal-like ^{57}Fe ENDOR spectra reported here reveal an even greater complexity to the structure of the FeMo-co cluster; they arise from at least five nonequivalent iron sites. The additional iron site detected in the Mössbauer measurements may represent a sixth nonequivalent site,[29] or one of the ENDOR sites may represent an approximately equivalent pair as suggested by the pattern at g_z'. The analysis of ENDOR spectra taken at fields across the EPR envelope will settle the number of distinct sites detectable by ENDOR. The two spectroscopic techniques give consistent results for the magnitudes and signs of the ^{57}Fe coupling constants, but the ability to obtain angle-resolved information by collecting ENDOR spectra at different observing fields has enabled us to detect and to begin quantitating the hyperfine tensor anisotropy. Examination of the data in Table II shows that the ^{57}Fe couplings for Avl and Kpl are quite similar and differ from those of Cpl. Moreover, analysis of the ^{57}Fe nuclear Zeeman splittings, in conjunction with analysis of the electronic g tensor, shows that Cpl also has ~20% smaller zero-field splitting.

The ENDOR data corroborate the Mössbauer results in indicating that the iron sites can be divided into two classes on the basis of their hyperfine coupling constants. The B-type sites have small, positive hyperfine couplings that preliminary analysis suggests to be rather closely isotropic, a characteristic suggestive of high-spin ferric ions. The A-type sites have larger, negative couplings that appear to be appreciably anisotropic, suggestive of high-spin ferrous ions. To the extent that these analogies to iron atoms in well-defined oxidation states apply in what must be a highly covalent system and may be confirmed by a subsequent full analysis of the hyperfine tensors, they can be used along with the results for molybdenum as a starting point for discussions of the cluster electronic structure.

The ^{57}Fe hyperfine couplings are reduced from the range exhibited by mononuclear high-spin Fe^{2+} or Fe^{3+} sites and show both positive and negative signs. These features are a signature of the spin coupling that produces the net $S = {}^3/_2$ cluster spin.[44,45] However, in the familiar [2Fe-2S], [3Fe-4S], and [4Fe-4S] centers, spin coupling to form a cluster spin $S = {}^1/_2$ produces at least one iron site with an A value larger than that in the uncoupled system. This is not the case with MoFe. The B- and A-site couplings in Table II may be compared, respectively, with the roughly 2-fold and 50% larger couplings for the two types of iron observed in oxidized HiPIP: $A \simeq 21$ MHz and $A \simeq 31$ MHz.[46] The $S = {}^3/_2$ $MoFe_3S_4$ cubane-type clusters[47] exhibit two types of irons having $A \simeq 15$ MHz and $A \simeq -11$ MHz and thus would appear to provide an interesting reference system for the magnitudes of the ^{57}Fe hyperfine couplings in MoFe.

An EPR-active ($S = {}^1/_2$) [FeS] cluster in oxidized bidirectional hydrogenase also has two types of iron sites with small A values: 9.5 and 17 MHz.[48] The absence of a large coupling was deemed anomalous, and the possibility of a sulfur-based radical was considered. That would not appear to be present here, however, as the ^{33}S ENDOR spectra of Cpl presented here show resonances from numerous sulfur sites with small hyperfine couplings. This is the pattern expected from the picture of FeMo-co as a covalent, spin-coupled metal center, and not for a center with significant localization of spin on sulfur, where coupling constants an order of magnitude larger are expected.[41]

As discussed above, several lines of argument suggest that the ligands attaching the FeMo-co cluster to the protein are predominantly, or even totally, associated with residues other than cysteine. Several approaches can be used to test the assignment of the ^{33}S resonances to S^{2-} ions. We shall examine the ^{33}S resonances of enriched ferredoxins obtained from the same culture that yielded the enriched MoFe; with fewer sulfurs, unambiguous assignments may be possible. In principle, it would be possible to simplify the ^{33}S ENDOR pattern of a ferredoxin or MoFe by extracting the ^{33}S-enriched metal center and inserting it into unenriched apoprotein. In this way resonances due to cysteine sulfurs would be eliminated, and only those from inorganic sulfur involved directly with the cofactor would remain. The reverse process also can be performed, using unenriched FeMo-co. Such experiments are planned, now that we have shown that resolved sulfur resonances can be detected from proteins with a low level of enrichment.

If we accept the arguments against cysteinyl coordination to the cofactor, then ENDOR measurements would *appear* to suggest by elimination that the FeMo-co cluster is linked to the protein by oxygen ligands as follows: Whereas our recent ^{14}N ENDOR measurements showed that the [2Fe-2S] cluster of the Rieske protein is in part bound to the protein by nitrogenous ligands,[39b] we have detected no resonances from the MoFe proteins that can be assigned to ^{14}N. However, our IR study of FeMo-co in NMF solutions[49] indicated that extracted factor is coordinated to deprotonated NMF, presumably through N. Moreover, weakly coupled nitrogen ($A \sim 1$-2 MHz) has been detected in the nuclear modulations of electron spin-echo decay curves,[50] and such weak couplings would be difficult to detect in ENDOR. Clearly, a parallel search for ^{14}N resonances in the MoFe proteins and in isolated cofactor is required before firm conclusions can be drawn as to the coordination of cofactor to the protein.

The most important conclusion to be drawn from the ENDOR observation of hyperfine couplings to molybdenum is that the molybdenum is indeed electronically integrated with the EPR-visible FeMo-co clusters. Previous studies of CW EPR spectra of MoFe proteins failed to give evidence of ^{95}Mo hyperfine broadening.[10] In addition, computer simulations of the EPR spectrum using the A^{Mo} determined by ENDOR support the conclusion that the cluster contains a single molybdenum at an upper limit and that the resting-state MoFe protein therefore contains two such centers. The small value of A^{Mo} indicates that the molybdenum is a nonmagnetic, even-electron ion with an even formal valency. This result, and a comparison of the ^{95}Mo quadrupole coupling to those estimated from ^{95}Mo NMR studies of mononuclear complexes, supports the assignments of an unsymmetrically coordinated Mo(IV) for molybdenum in the resting-state MoFe protein, which focuses interest on synthetic monomolybdenum–iron–sulfur complexes where Mo is in intermediate oxidation states.

Acknowledgment. We thank Prof. J. H. Enemark for stimulating conversations and for informing us of unpublished results. This work was supported by Grants PCM 8350218 (B.M.H.) and PCM 8205764 (W.H.O.-J.) from the National Science Foundation Biophysics Program, by the Petroleum Research Fund, administered by the American Chemical Society (B.M.H.), and by Grant 84-CRCR-1-1407 from the USDA (W.H.O.-J.). The ENDOR spectrometer was purchased with a grant from the NSF Biological Instrumentation Program (PCM-8116106) and received support from the Northwestern University Materials Research Center under the NSF-MRC Program (DMR 8216972).

Registry No. ^{57}Fe, 14762-69-7; ^{95}Mo, 14392-17-7; ^{33}S, 14257-58-0.

(44) Sands, R. H.; Dunham, W. R. *Q. Rev. Biophys.* **1975**, *7*, 443–504.
(45) Kent, T. A.; Huynh, B. H.; Münck, E. *Proc. Natl. Acad. Sci. U.S.A.* **1980**, *77*, 6574–6576.
(46) (a) Middleton, P.; Dickson, D. P. E.; Johnson, C. E.; Rush, J. D. *Eur. J. Biochem.* **1980**, *104*, 289–296. (b) Anderson, R. E.; Anger, G.; Petersson, L.; Ehrenberg, A.; Cammack, R.; Hall, D. O.; Mullinger, R.; Rao, K. K. *Biochim. Biophys. Acta* **1975**, *376*, 63–71.
(47) Mascharak, P. K.; Papefthymoiu, G. C.; Armstrong, W. H.; Foner, S.; Fraenkel, R. B.; Holm, R. H. *Inorg. Chem.* **1983**, *22*, 2851–2858.
(48) Wang, G.; Benecky, M. J.; Huynh, B.-H.; Cline, J. F.; Adams, M. W. W.; Mortenson, L. E.; Hoffman, B. M.; Münck, E. *J. Biol. Chem.* **1984**, *259*, 14328–14331.
(49) Walters, M. A.; Chapman, S.; Orme-Johnson, W. H. *Polyhedron*, in press.
(50) Orme-Johnson, W. H.; Mims, W. B., unpublished results.